FREESTREAM-TURBULENCE INDEPENDENCE OF SECONDARY INSTABILITY OF CROSS-FLOW VORTICES IN SWEPT-FLAT-PLATE BOUNDARY LAYER

Kosuke Nakagawa
Department of Mechanical Engineering
Tokyo University of Science
2641 Yamazaki, Noda-shi, Chiba, 278-8510
7522702@ed.tus.ac.jp

Takahiro Ishida
Aeronautical Technology Directorate
Japan Aerospace Exploration Agency (JAXA)
6-13-1 Osawa, Mitaka, Tokyo 181-0015
ishida.takahiro@jaxa.jp

Takahiro Tsukahara
Department of Mechanical Engineering
Tokyo University of Science
2641 Yamazaki, Noda-shi, Chiba, 278-8510
tsuka@rs.tus.ac.jp

ABSTRACT

Laminar-to-turbulent transition on a swept-flat plate is caused by the breakdown of the cross-flow vortex via the high-frequency secondary instability. In order to determine common transition mechanisms, this parametric study has analyzed turbulent transitions under various environmental conditions including wall-roughness elements and freestream turbulence. We performed direct numerical simulations of the Falkner–Skan–Cooke boundary layer with various conditions of isolated roughness and/or different peak wavelengths of freestream turbulence. In the roughened case, where the flow was accompanied by the stationary cross-flow vortex, the short-wavelength freestream turbulence promoted the secondary instability with hairpin vortices, while the long-wavelength disturbance delayed the cross-flow-vortex break down compared to the short wavelength condition. The wavelength of freestream disturbance played a key role to promote high-frequency secondary instability on the cross-flow vortex. The main finding here is, with or without freestream turbulence, the high-frequency secondary instability is commonly the trigger for the breakdown to turbulence.

INTRODUCTION

A swept wing has a backward angle against the fuselage. Near its leading edge, the cross-flow instability is dominant and promotes the turbulent transition. The cross-flow instability forms a cross-flow vortex. As the cross-flow vortex evolves downstream, the turbulent transition is induced after a nonlinear saturation. At the saturation state, a high-frequency disturbance called secondary instability occurs. The high-frequency secondary instability is the main factor of the turbulent transition of the cross-flow vortex. A cross-flow vortex via the surface roughness forms a stationary vortex, while a traveling vortex via environmental disturbance such as freestream turbulence (FST), or both, may occur. The crossover of stationary and traveling vortices is still unclear. The interaction of roughness and freestream disturbance should be clarified.

Brynjell-Rakola et al. (2017) simulated flows past an isolated cylindrical roughness, which is a kind of surface roughness, on the swept-flat plate by direct numerical simulation. They investigated the turbulent transition process of the stationary cross-flow vortex. They also detected the location of high-frequency secondary instability on the cross-

flow vortex. Högberg & Henningson (1998) reported that the frequency ω of secondary instability was the order of 10^0. The frequency was non-dimensionalized by the external chordwise velocity U_0 and the displacement thickness δ^*. The high-frequency secondary instability was classified into y- and z-type modes, based on the relative position against the cross-flow vortex. These frequencies were found to be unstable for the cross-flow vortices (Brynjell-Rakola et al., 2015; 2017).

Many studies reported that the FST modulated the stationary cross-flow vortex, and induced a traveling vortex. Deynhel & Bippes (1996) performed a wind-tunnel test on the swept-flat-plate model under various FST intensity conditions. They found that the threshold of FST intensity Tu, above which the traveling vortex dominates the turbulent transition process. The threshold was approximately 0.2%. Downs & White (2013) showed the effects of FST on the stationary mode and unstable modes of the cross-flow vortices by wind tunnel tests. The unstable disturbances were intensified by the FST.

Although the turbulent transition process via the isolated roughness elements and the intensity of the FST have been studied, there is less understanding of the interaction between the stationary vortex (due to a wall roughness) and the FST. There are few studies on the effects of the wavelength distribution of the FST. In this study, we focused on the peak wavelength of the FST and compare the turbulent transition processes depending on the characteristics of the FST alone and the interaction with the stationary cross-flow vortex which is induced by the cylindrical roughness. We aimed to obtain critical conditions of the transition process related to the cross-flow vortex that is exposed to FST by discussing the turbulent transition process.

NUMERICAL METHOD

The base flow was Falkner–Skan–Cooke (FSC) similarity solution (Brynjell-Rakola et al., 2017). We performed DNS of incompressible three-dimensional boundary-layer flows. The governing equations are the continuity and the Navier–Stokes equations. The computational domain was $(L_x \times L_y \times L_z) = 200$–$800\delta_0^* \times 25.14\delta_0^* \times 27\delta_0^*$ in the chordwise (x), spanwise (y), and wall-normal (z) directions, respectively. Here, δ_0^* is the displacement thickness at the inlet of the computational domain. The number of grids was 1024–4096 × 128 × 128. A periodic boundary condition was imposed in the y- direction, and the non-slip condition was applied at the wall. In the x- direction, the convective outflow condition was applied. The cylindrical

roughness with a height of k_z and a diameter of $6.0\delta_0^*$ was implemented by an immersed boundary method, and its center was located at $x/\delta_0^* = 20.59$. The spanwise roughness spacing of $25.14\delta_0^*$ corresponds to the most unstable stationary cross-flow mode. The Reynolds number Re ($= U_0\delta_0^*/\nu$) was 337.9, where U_0 is the external chordwise velocity at the inlet. The details of the numerical method were reported in our previous paper (Ishida et al., 2022). Validation carried out is discussed in the next section.

The method of simulating freestream turbulence (FST) was referred to as Watanabe & Maekawa (2015), allowing us to select arbitrarily a turbulent intensity (Tu) and a peak wavelength (λ_{max}/δ_0^* ($=L_y/\delta_0^*/k$)). The energy spectrum of FST is given as

$$E(\boldsymbol{k}) = \boldsymbol{k}^4 \exp(-2(\boldsymbol{k}/k_{max})^2). \qquad (1)$$

Figure 1 shows the energy spectrum for different peak wavelengths. The turbulence intensity of the disturbance is defined as $Tu = (u_i^2/3)^{1/2}\times100[\%]$, where u_i indicates the disturbance velocity. In this study, we fixed $Tu = 0.1$ %. The disturbance was damped in the near-wall region at the inlet according to the shape of the chordwise FSC velocity profile to satisfy the non-slip condition.
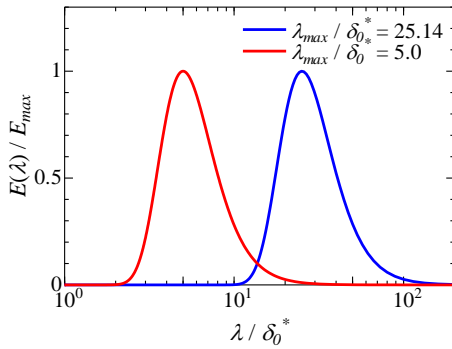

Figure 1. Energy spectrum for freestream turbulence.

RESULTS

First, we demonstrate diverse phenomena in the turbulent transition processes depending on the cylindrical roughness and the freestream turbulence (FST). Figure 2 shows the chordwise distribution of the friction coefficient, C_f. Upstream, the friction coefficients are close to the laminar value of the FSC flow. Downstream, the friction coefficients drastically increase. The increase is owing to the proceeding of the transition process. Under the roughness condition, the turbulent transition is much earlier at $x/\delta_0^* \approx 100$ in the short-wavelength condition of $\lambda_{max}/\delta_0^* = 5.0$. Högberg & Henningson (1998) reported a high-frequency secondary instability on the shear layer after cross-flow vortex saturation. As in the present result, the stationary cross-flow vortex near the wake of cylindrical roughness is forced to have a high-frequency secondary instability by the high-frequency disturbance of the FST. Therefore, the turbulent transition in the short-wavelength condition occurs earlier than in the long-wavelength and no-FST conditions. On the other hand, without roughness, the long-wavelength condition of $\lambda_{max}/\delta_0^* = 25.14$ causes an early turbulent transition. In this case, the cross-flow vortex is absent for a long extent and, of course, the secondary instability should not emerge in this range. In the long-wavelength condition, the peak wavelength corresponds to the most unstable stationary cross-flow mode ($\lambda/\delta_0^* = 25.14$),

inducing a cross-flow vortex earlier than in the short-wavelength condition. From the comparison between the roughness condition and without roughness condition, the stationary or traveling cross-flow vortex is necessary for the early transition process via the FST-induced secondary instability.
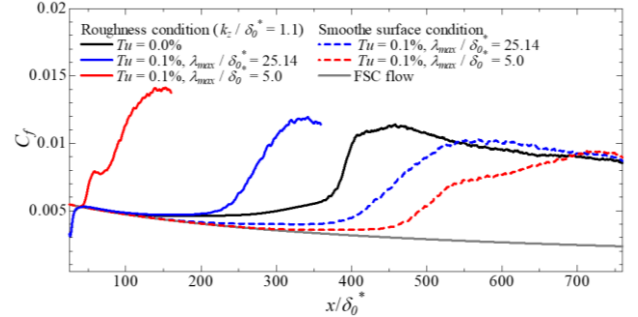

Figure 2. Friction coefficient distribution.

Figure 3 shows the visualizations of vortex structures for the only cylindrical roughness case and the only FST case. The vortex structure is visualized by the iso-surface of the second invariant of the velocity gradient tensor Q and colored by $u'w'/U_0^2$. The vortex emerges at the increasing position of the friction coefficient plotted in Fig. 2. These are the finger vortex via the high-frequency secondary instability. The vortex structures are the same as those reported by Brynjell-Rahkola et al. (2017) and Wassermann & Kloker (2003) and are the typical structure that can be observed in the turbulent transition
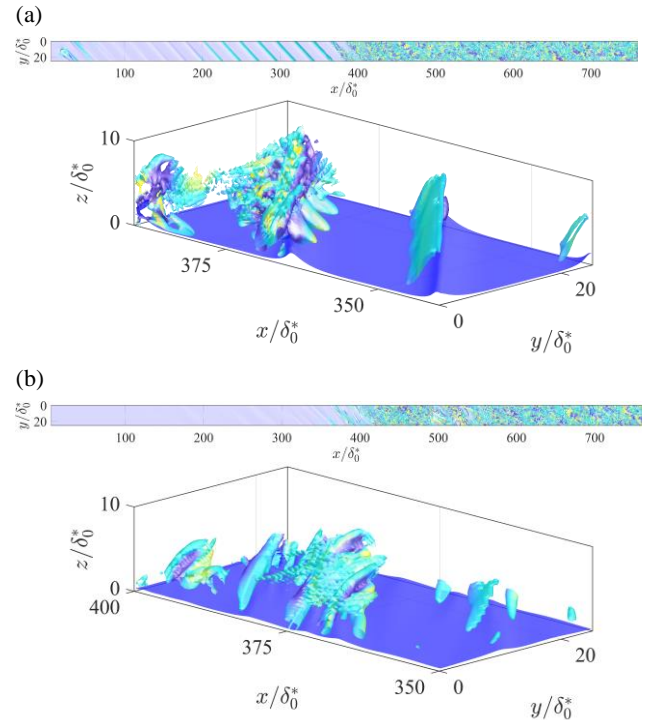
(a)

(b)

Figure 3. Visualization for instantaneous vortex structure colored by $u'w'/U_0^2$ between -0.015 (blue) to 0.015 (red). Iso-surfaces are $u/U_0 = 0.3$ (blue) and $Q = 0.005$. Bottom figure is enlarged view of the finger vortex. (a) shows the condition of $k_z/\delta_0^* = 1.1$ and $Tu = 0.0$ %. (b) shows the condition without roughness, but with long-wavelength freestream turbulence ($Tu = 0.1$ %, $\lambda_{max}/\delta_0^* = 25.14$).
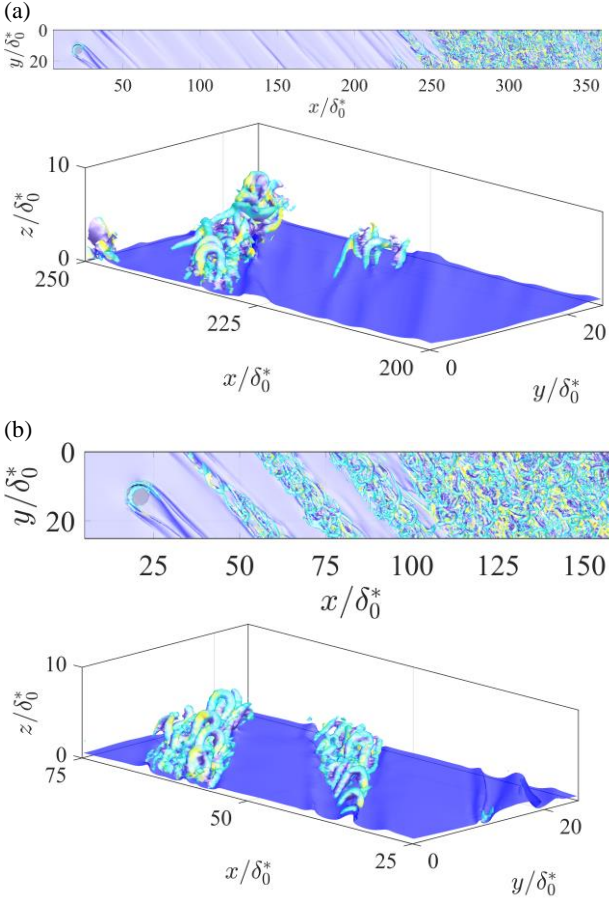
Figure 4. Visualization for instantaneous vortex structure of freestream turbulence condition (Tu = 0.1 %). Iso-surfaces and color are same as Fig. 3 but Q = 0.05. (a) shows the long-wavelength condition (λ_{max}/δ_0^* = 25.14) and k_z/δ_0^* = 1.1. (b) shows the short-wavelength condition (λ_{max}/δ_0^* = 5.0) and k_z/δ_0^* = 1.1.

processes in this case. The finger vortex has $u'w' < 0$ regions. It suggests the onset of Reynolds shear stress. Under the case of the roughness and FST, there are different vortex structures. Figure 4 shows the flow fields with the same iso-surfaces as Fig. 3. Under the short-wavelength case, hairpin vortices occur near the wake of roughness. Hairpin vortices provide the wake vortex with the transition to turbulence via high-frequency secondary instability. The hairpin vortex has a sweep and ejection region, where fluid motions of blowing down and up around the vortex, respectively (Robinson; 1991), resulting in $u'w' < 0$. The characteristics of fluid motions are the same as the finger vortex. Under the long-wavelength condition, the formation of the finger vortex is the same as in Fig. 3. There are also fluid motions of $u'w' < 0$ around the finger vortex. In addition, the correspondence with the friction coefficient distribution (Fig. 2) indicates that vortices are the trigger of turbulent transition.

We show the common characteristics between the hairpin and finger vortexes, which are induced by the high-frequency secondary instability in the swept-flat-plate boundary layer, by means of the frequency analysis of the disturbance velocity components. In the frequency analysis, the sampling period Δt^* and averaging time T^* equal 0.098 and 390, respectively. Measurement positions are at the secondary vortices shown in Figs. 3 and 4. Figure 5(a) shows the frequency analysis with

roughness condition, where we aim to extract the frequencies of the hairpin and finger vortexes. The frequency of the high-frequency instability reported by Högberg & Henningson (1998) was $\omega \approx 0.9$. Brynjell-Rahkola et al. (2015) reported the frequency of the unstable fluctuations at the cross-flow vortex, which was $\omega \gtrsim 0.9$. Our results shown in Fig. 5(a) indicate that the frequency of the secondary instability are independent of the secondary vortex structure: both two cases exhibit a peak at ω = 0.6–0.9, which correspond to that of the previous studies. Figure 5(b) shows the case with long-wavelength FST, in which there only occurs the finger vortex. In this case, low-frequency disturbances occur most strongly which is consistent with a report by Högberg & Henningson (1998). This spectrum implies strong growth for a traveling wave. Owing to the spanwise advection characteristic of traveling waves, the frequency of secondary instability becomes low. However, independently of the FST wavelength, the secondary vortex provides the stationary vortex with an increase in the high-frequency disturbance.
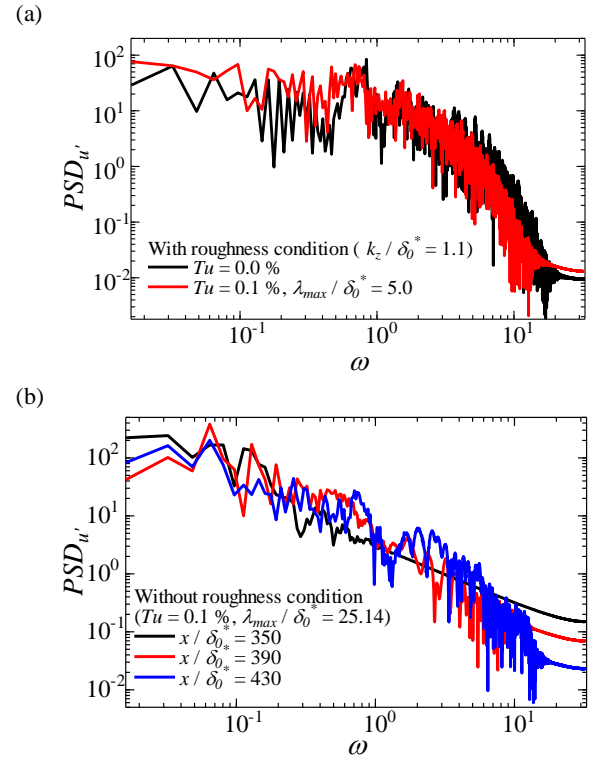
(a)

(b)

Figure 5. Frequency analysis of chordwise disturbance velocity (u'/U_0). (a) shows independency on secondary vortex structure with roughness condition (k_z/δ_0^* = 1.1). Black: obtained at $(x, y, z)/\delta_0^* \approx (370, 2.6, 2.4)$. Red: $(x, y, z)/\delta_0^* \approx (50, 14.5, 1.0)$. (b) shows without roughness condition for λ_{max}/δ_0^* = 25.14 at $(y, z)/\delta_0^* \approx (10.0, 2.4)$.

From these results, we clarified that the turbulent transition of the swept-flat-plate boundary layer proceeds through the hairpin vortex or finger vortex owing to the high-frequency secondary instability at the shear layer. This is a feature common to all the transition processes, independent of the surface roughness and FST conditions.

CLYRINDRICAL ROUGHNESS HEIGHT

Under conditions of cylinder roughness and FST, we found that the vortex structures and turbulent transition positions
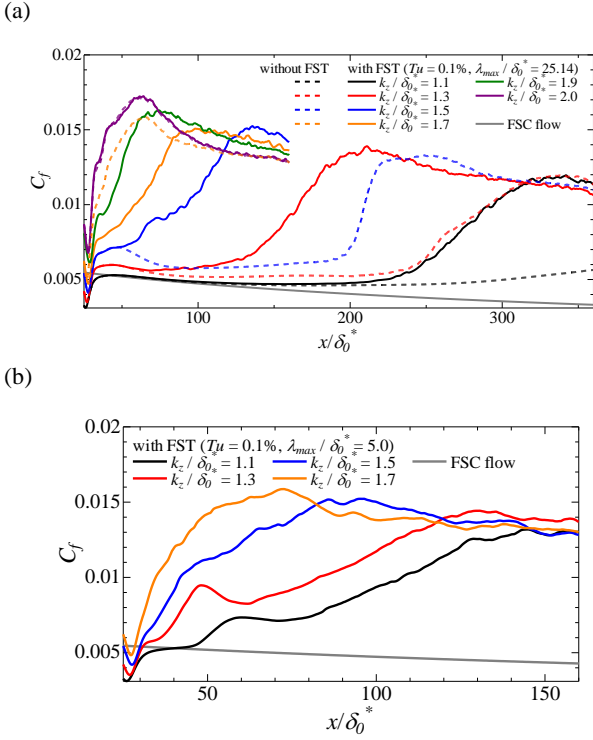
3

(a)

(b)

Figure 6. Friction coefficient distribution. (a) shows long-wavelength conditions and no freestream turbulence conditions. (b) shows short-wavelength conditions.

differ depending on the wavelength of the FST. We investigate the dependence of secondary vortex structures and transition positions on the height of the cylinder roughness.

Figure 6 shows the friction coefficient distribution for different cylinder roughness heights. In the no-FST condition, the transition position shifts upstream as the cylinder roughness height increases. The same is observed under conditions with FST. With long-wavelength FST, the transition position shifts upstream with increasing height are not remarkable in $k_z/\delta_0^* \geq$ 1.5 than in $k_z/\delta_0^* < 1.5$. In the high roughness height condition, the influence of the roughness-induced disturbance dominates the turbulent transition process. Figure 7 shows the flow field for the roughness height $k_z/\delta_0^* = 1.5$ in the long-wavelength condition. Hairpin vortices occur near the roughness. Note, the secondary vortex is a finger vortex with $k_z/\delta_0^* = 1.1$ (see Figure 4(a)). The secondary vortex inducing the turbulent transition changed to a hairpin vortex as the roughness height increased (see figure 7). The low roughness results ($k_z/\delta_0^* = 1.1$) show that the switch of secondary vortex structure between hairpin and finger vortices depends on the FST wavelength. However, the roughness-height study clarified that both the cylindrical roughness height and the FST wavelength affect the switch of secondary vortex structure. Although many factors affect the transition process, they undergo the secondary instability.

Finally, we focus on the disturbance components occurring on the stationary cross-flow vortices and discuss them from the turbulent energy production. The production terms are the following:

$P_k1 = -u'^2 \partial u/\partial x$, $P_k2 = -u'w' \partial u/\partial z$, $P_k3 = -u'v' \partial u/\partial y$,
$P_k4 = -u'w' \partial w/\partial x$, $P_k5 = -w'^2 \partial w/\partial z$, $P_k6 = -v'w' \partial w/\partial y$,
$P_k7 = -u'v' \partial v/\partial x$, $P_k8 = -v'w' \partial v/\partial z$, $P_k9 = -v'^2 \partial v/\partial y$,
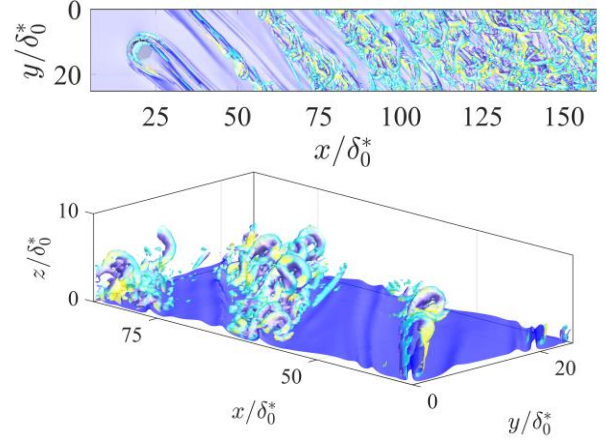$P_k = P_k1 + P_k2 + \ldots + P_k9$.　　　　(2)

Figure 7. Top view for the short-wavelength condition of k_z/δ_0^* = 1.5. Isosurfaces are same as Fig. 4.

The fluctuation component is determined as $u'/U_0 = u/U_0 - \bar{u}/U_0$, where $\bar{u}$ is the time-averaged component. Figure 8 shows the contribution of each production term to the turbulent transition. Under no-FST conditions, P_k2, P_k8, and P_k9 take a dominant role in the production. Among these, P_k2 and P_k8 are the production terms that provide $u'w'$ and $v'w' < 0$. These correspond to the finger vortex shown in Fig. 3. The highest contribution of P_k9 is caused by the fluctuation induced by the finger vortex and the spanwise velocity gradient. The grown cross-flow vortex provides a minimum velocity gradient with a flow field. Malik et al. (1999) called this velocity gradient as mode z, which is one of the secondary instability modes. In other words, P_k9 increases with the growth and saturation of the cross-flow vortex. That is a characteristic trend of the turbulent transition conditions caused by the finger vortex. According to Vincentiis et al. (2022), for a swept-wing boundary layer, the production term of the spanwise velocity gradient takes a dominant role in the turbulence transition. For the two-dimensional flow (Loiseau et al., 2014), the dominant production term was also owing to the spanwise velocity gradient, which was created by the cylindrical roughness.

Figure 9 shows the contribution of the production term under the FST condition. Comparing the no-FST condition (Fig. 8) and the short-wavelength FST condition (Fig. 9(a)), the contributions of Pk2 and Pk8 are more significant in the short-
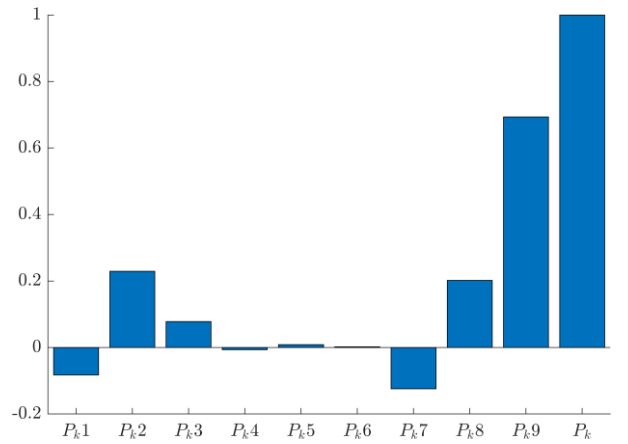

Figure 8. Contribution to the integral value of production terms scaled by P_k of $k_z/\delta_0^* = 1.1$. The integral region is $x \in [25, 400]$, $y \in [0, 25.14]$, $z \in [0, 10]$.
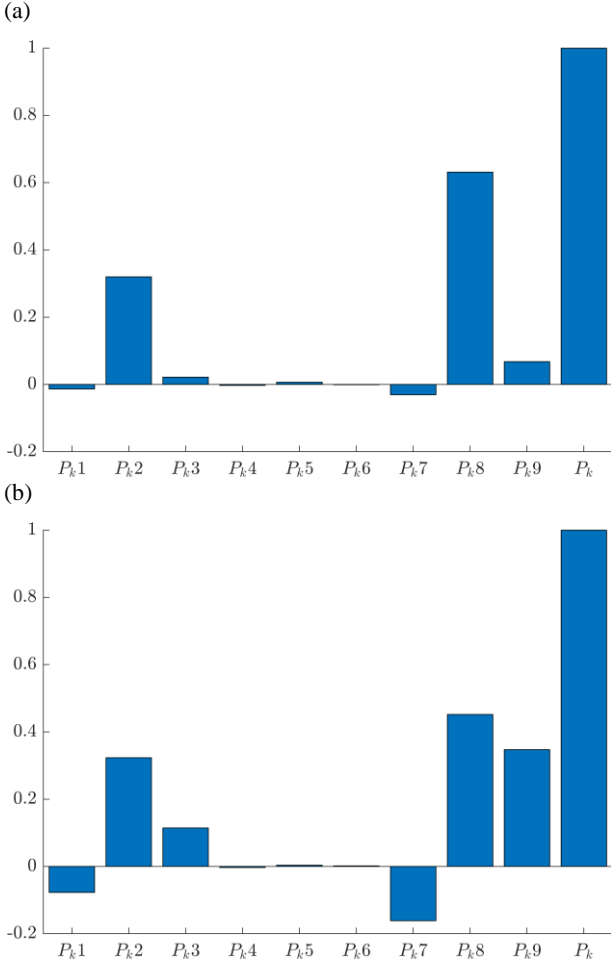
(a)

(b)

Figure 9. Contribution to the integral value of production terms scaled by P_k of $k_z/\delta_0^* = 1.1$. (a) is short-wavelength condition. The integral region is $x \in [25, 150]$, $y \in [0, 25.14]$, $z \in [0, 10]$. (b) is long-wavelength condition. The integral region is $x \in [25, 300]$, $y \in [0, 25.14]$, $z \in [0, 10]$.

wavelength condition. The sweep/ejection by the hairpin vortex induces P_k2 and P_k8. The short-wavelength FST provides a stationary vortex with a secondary vortex earlier. Near the cylinder roughness, the spanwise velocity gradient is low. The P_k9 is also lower than the grown cross-flow vortex. With the long-wavelength FST (Fig. 9(b)), the contributions of P_k2, P_k8, and P_k9 are comparable. In this case, the finger vortex induces turbulent transition. It is the same as no-FST conditions. However, compared to the no-FST condition, the transition occurs upstream (see Fig. 2). The contribution of P_k9 is lower owing to the cross-flow vortex growth. The contributions of P_k2 and P_k8 are common to all conditions, irrespective of the FST. The generation of turbulence energy by P_k2 and P_k8 are a characteristic feature for the system in the cross-flow instability dominant. However, the contribution rate of P_k differs under different conditions. It is due to the growth of the cross-flow vortex.

Figure 10 shows the dependence of the integral value of the production term (P_k) on roughness height and FST wavelength. The black line in Fig.10 is based on the results of production terms and the secondary vortex structures of the flow field. The clear threshold between secondary vortices is not yet evident. In the chordwise region $x/\delta_0^* < 150$, the hairpin vortex provides high value of P_k. However, under the conditions of turbulent

transition via the finger vortex, the fluctuation component is low within $x/\delta_0^* < 150$ (see figure 4(a)). Therefore, turbulent production is also low. It is possible to classify the secondary vortex structures by the turbulent production near the cylinder. The classification by production term is the same as the observations of the vortex structures in the flow field.
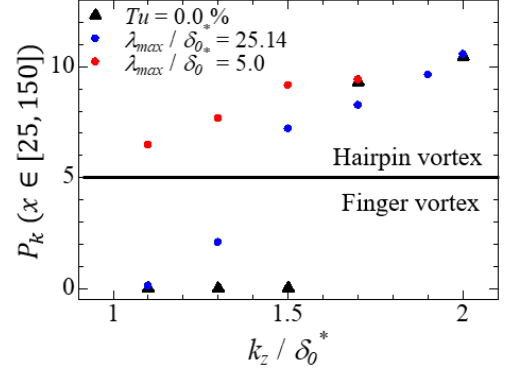

Figure 10. Roughness height and wavelength dependency of integral value of production term. The integral region is $x \in [25, 150]$, $y \in [0, 25.14]$, $z \in [0, 10]$.

SUMMARY

We performed direct numerical simulations for turbulent transitions in a swept-flat-plate boundary layer with isolated cylinder roughness and the freestream turbulence (FST). We investigated the similarities/differences between secondary vortices via the high-frequency instability.

The stationary cross-flow vortex paths the growth, saturation, and breakdown. In the saturation term, high-frequency secondary instability induces the finger vortex on the cross-flow vortex. The FST induces secondary instability earlier than the no-FST condition. In short-wavelength FST conditions, high-frequency secondary instabilities occurred immediately after the roughness. It provided hairpin vortices. In the long-wavelength FST condition, the finger vortexes occurred earlier than in the no-FST condition. FST skipped the saturation term and produced secondary instability. In the without roughness condition, FST induces a traveling cross-flow vortex. The traveling cross-flow vortex is also breakdown via high-frequency secondary instability. As a unified result of different conditions, the turbulent transition process follows a path of velocity shear layer formation. At the late stage of the transition process, the flow field becomes breakdown owing to secondary instability. The increasing roughness height changed only the secondary vortex structure. An analysis of the production terms clearly shows that the dominant production term differs depending on the secondary vortex structure. The production term with spanwise velocity gradient changes significantly concerning the growth of the cross-flow vortex. These differences depend on the presence/absence of a saturation term of the cross-flow vortex. However, the production terms related to the secondary vortex are similar.

ACKNOWLEDGEMENT

REFERENCES

Brynjell-Rahkola, M., Schlatter, P., Hanifi, A. and Henningson, D.S., 2015 "Global stability analysis of a roughness wake in a Falkner-Skan-Cooke boundary layer", *Procedia IUTAM*, Vol. 14, pp. 192-200.

Brynjell-Rakola, M., Shahriari, N., Schalatter, P., Hanifi, A. and Henningson, D. S., 2017, "Stability and sensitivity of a cross-flow-dominated Falkner-Skan-Cooke boundary layer with discrete surface roughness", *Journal of Fluid Mechanics*, Vol. 826, pp. 830-850.

Deyhle, H. and Bippes, H., 1996, "Disturbance growth in an unstable three-dimensional boundary layer and its dependence on environmental conditions", *Journal of Fluid Mechanics*, Vol. 316, pp. 73-113.

Downs, R.S. and White, E.B., 2013, "Free-stream turbulence and the development of cross-flow disturbances", *Journal of Fluid Mechanics*, Vol. 735, pp. 347-380.

Högberg, M. and Henningson, D., 1998, "Secondary instability of cross-flow vortices in Falkner-Skan-Cooke boundary layer", *Journal of Fluid Mechanics*, Vol. 368, pp. 339-357.

Ishida, T., Tsukahara, T., and Tokugawa, N., 2022, "Parameter effects of spanwise-arrayed cylindrical roughness elements on transition in the Falkner-Skan-Cooke boundary layer," *Transactions of the Japan Society for Aeronautical and Space Sciences*, Vol. 65, pp. 84-94.

Loiseau, J-C., Robinet, J-C., Cherubini, S., and Leriche, N., 2014, "Investigation of the roughness-induced transition: global stability analyses and direct numerical simulations", *Journal of Fluid Mechanics*, Vol. 760, pp. 175-211.

Malik, M.R., Li, F., Choudhari, M.M., and Chang, C-L., 1999, "Secondary instability of crossflow vortices and swept-wing boundary-layer transition", *Journal of Fluid Mechanics*, Vol. 399, pp. 85-115.

Robinson, S.K., 1991, "Coherent motions in the turbulent boundary layer", *Annual Review of Fluid Mechanics*, Vol. 23, pp. 601-639.

Vincentiis, L.D., Henningson, D.S., and Hanifi, A., 2022, "Transition in an infinite wept-wing boundary layer subject to surface roughness and free-stream turbulence", *Journal of Fluid Mechanics*, Vol. 931, A24, 27 pages.

Wassermann, P. And Kloker, M., 2003, "Transition mechanisms induced by travelling crossflow vortices in a three-dimensional boundary layer", *Journal of Fluid Mechanics*, Vol. 483, pp. 67-89.

Watanabe, D. and Maekawa, H., 2015, "Rapid growth of unsteady finite-amplitude perturbations in a supersonic boundary-layer flow," *International Symposium on Turbulent and Shear Flow Phenomena*, Vol. 3B-4, 6 pages.